Assessment of the conjunctival microcirculation in adult patients with cyanotic congenital heart disease compared to healthy controls

Title Page

Manuscript title Assessment of the conjunctival microcirculation in adult patients with cyanotic congenital heart disease compared to healthy controls

Author list (in order)

1. Dr Paul F. Brennan[1,2]
2. Dr Min Jing[4]
3. Dr Andrew J. McNeil[2]
4. Miss Agnes Awuah[2]
5. Dr Jonathan Mailey[1]
6. Dr Bronagh Kelly[1]
7. Professor Dewar D. Finlay[4]
8. Professor Kevin Blighe[2]
9. Professor James A.D McLaughlin[4]
10. Dr M. Andrew Nesbit[2]
11. Professor EmanueleTrucco[3]
12. Dr Christopher J. Lockhart[1]
13. Professor Tara C.B. Moore[2]
14. Dr Mark S. Spence[1]

Corresponding author Dr Paul Brennan[1]

paul.brennan@belfasttrust.hscni.net

Institutions *[1] Department of Cardiology, Royal Victoria Hospital, Belfast Health and Social Care Trust, Belfast, United Kingdom*

[2] Biomedical Sciences Research Institute, Ulster University, Coleraine, United Kingdom

[3] VAMPIRE project, Computing (SSEN), University of Dundee, Dundee, United Kingdom

[4] Nanotechnology and Integrated Bioengineering Centre (NIBEC), Ulster University, Jordanstown, United Kingdom

Wordcount 4978 words (excluding abstract, funding, acknowledgements, competing interests and references)

Funding This project was funded by the Heart Trust fund, Royal Victoria Hospital, Belfast; the Regional Medical Cardiology Centre (RMCC), Royal Victoria Hospital, Belfast; Northern Ireland Chest Heart and Stroke (NICHS) and the Ulster University located in Northern Ireland, United Kingdom. The work for image processing and microcirculatory parameters estimation was part-funded by Interreg SEUPB funding associated with Eastern Corridor for Medical Engineering (ECME).

Abstract

Purpose Congenital heart disease (CHD) is the most common live birth defect and a proportion of these patients have chronic hypoxia. Chronic hypoxia leads to secondary erythrocytosis resulting in microvascular dysfunction and increased thrombosis risk. The conjunctival microcirculation is easily accessible for imaging and quantitative assessment. It has not previously been studied in adult CHD patients with cyanosis (CCHD).

Methods We assessed the conjunctival microcirculation and compared CCHD patients and matched healthy controls to determine if there were differences in measured microcirculatory parameters. We acquired images using an iPhone 6s and slit-lamp biomicroscope. Parameters measured included diameter, axial velocity, wall shear rate and blood volume flow. The axial velocity was estimated by applying the 1D+T continuous wavelet transform (CWT). Results are for all vessels as they were not sub-classified into arterioles or venules.

Results 11 CCHD patients and 14 healthy controls were recruited to the study. CCHD patients were markedly more hypoxic compared to the healthy controls (84% vs 98%, p= 0.001). A total of 736 vessels (292 vs 444) were suitable for analysis. Mean microvessel diameter (D) did not significantly differ between the CCHD patients and controls (20.4 ±2.7μm vs 20.2 ±2.6μm, p=0.86). Axial velocity (Va) was lower in the CCHD patients (0.47 ±0.06mm/s vs 0.53 ±0.05mm/s, p=0.03). Blood volume flow (Q) was lower for CCHD patients (121 ±30pl/s vs 145 ±50pl/s, p=0.65) with the greatest differences observed in vessels >22μm diameter (216 ±121pl/s vs 258 ±154pl/s, p=0.001). Wall shear rate (WSR) was significantly lower for the CCHD group (153 ±27s^{-1} vs 174 ±22s^{-1}, p=0.04).

Conclusions This iPhone and slit-lamp combination assessment of conjunctival vessels found lower axial velocity, wall shear rate and in the largest vessel group, lower blood volume flow in chronically hypoxic patients with congenital heart disease. With further study this assessment method may have utility in the evaluation of patients with chronic hypoxia.

1. Introduction

Congenital heart disease (CHD) is the most common live birth defect, affecting nine in 1000 babies born in the UK (Bejal et al., 2016). Global prevalence of adult congenital heart disease (ACHD) patients is estimated at 3 per 1000 (Mulder et al, 2012). CHD lesions can be classified based on the presence or absence of cyanosis caused by deoxygenated haemoglobin concentration in the circulation leading to a bluish discolouration of the skin or mucous membranes (Baumgartner et al., 2010). Cyanotic congenital heart disease (CCHD) can occur early in life due to intra-cardiac shunts, obstruction to pulmonary blood flow or diminished pulmonary blood flow (Ossa et al., 2019; Waldman et al., 1999). Advancements in treatments have resulted in improved life expectancy for CCHD patients with nearly 90% of patients surviving into adulthood (Spence et al., 2007; Moons et al, 2010). Many of these patients tolerate chronic hypoxia and have measurable peripheral oxygen saturations at levels lower than non-cyanotic patients.

The objective of this study was to evaluate the effects that chronic hypoxia has on the conjunctival microcirculation of CCHD patients compared to a group of age and sex-matched healthy volunteers. The conjunctival microcirculation is readily-accessible and has been studied in healthy volunteers using a slit-lamp biomicroscope combined with either a smartphone (Brennan et al., 2019) or a digital charged camera device (Khansari et al., 2016;

Shahididi et al., 2010; Koutsiaris et al., 2007). Conjunctival microvascular assessment has been reported in patients with ischaemic stroke (Kord Valeshabad et al., 2015), diabetes mellitus (Khansari et al., 2017) and systemic hypertension (To et al., 2013). Changes in conjunctival blood flow velocity (Moka et al., 2019) have been reported in pregnant women.

Abnormalities in the retinal microcirculation have been reported in CCHD patients (Tsui et al., 2009; Cordina et al., 2015; Cordina et al., 2015_2). Non-invasive oximetry of the conjunctival and episcleral vessels have been assessed in patients with acutely induced mild hypoxia (FiO2 15% (Mackenzie et al., 2016)). To date, there are no reports describing slit-lamp assessment of the conjunctival microcirculation in CCHD patients.

2. Materials and methods

2.1 Subjects

This research study (IRAS 166742) was approved by the Research and Development review boards of the Ulster University (UU) and the Belfast Health and Social Care Trust (BHSCT). All subjects were provided with verbal and written information before study enrolment. Written consent was obtained from all patients and this study adhered to the Declaration of Helsinki.

CCHD patients were screened for eligibility at outpatient clinics and inpatient wards. Inclusion criteria for the CCHD patients required a history of chronic hypoxia secondary to CHD. Exclusion criteria included inability to consent, prior myocardial infarction (MI), uncontrolled systemic hypertension, recent history of conjunctival inflammation, prior refractive surgery, use of ocular medications (other than artificial tears) and current use of contact lenses.

Baseline clinical characteristics were obtained via the recruitment questionnaire and Northern Ireland Electronic Care Record (NIECR). We performed resting pulse oximetry and non-invasive blood pressure assessment at the time of conjunctival analysis.

2.2 Image acquisition

Conjunctival images were acquired using a Topcon SL-D4 (Topcon Medical Systems Inc., USA), an iPhone 6s smartphone (Apple, Inc, USA) and a bespoke adapter (Zarf Enterprises Inc., USA) as illustrated in **Figure 1.** An optimal configuration was set at a resolution of 1920×1080 pixels (p), captured at 60 frames per second. Using the third-party application "ProMovie Recorder" (www.promovieapp.com) we locked the video zoom setting at 2x, providing a 1:1- pixel mapping of the camera sensor at 1080p resolution. We acquired 5-10 second videos of the conjunctival microcirculation medial and lateral to the iris, generating four videos per subject. An external fixation target was used to minimise eye motion.

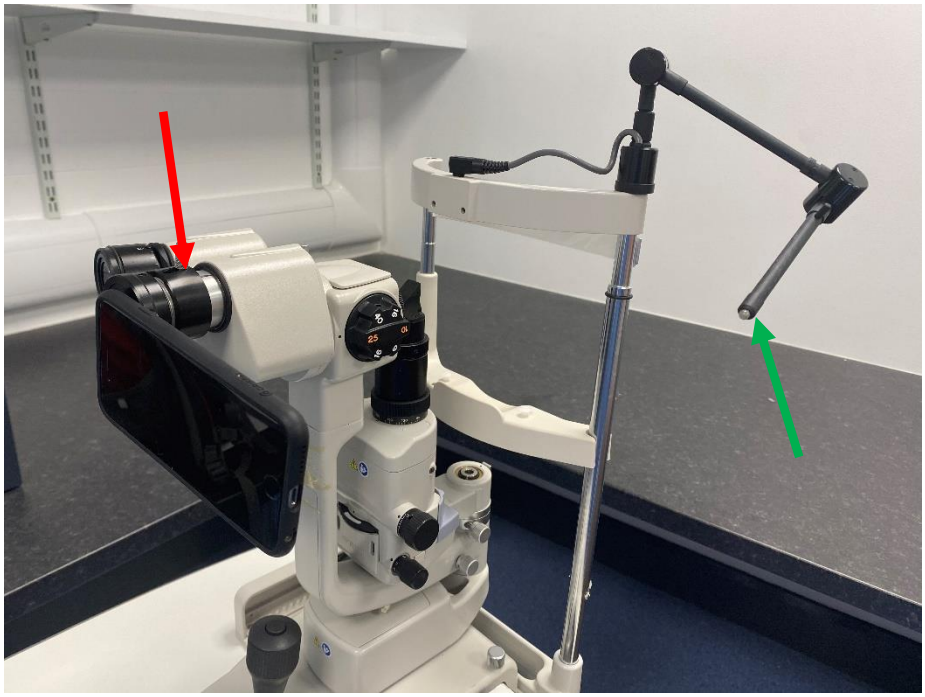

Figure 1. *The iPhone 6s, TopCon SL-D4 imaging system with the Zarf bespoke adapter (red arrow) and TopCon external fixation target (green arrow).*

2.3 Image processing

MALTAB R2019b (MathWork, USA) was used for programming. For video frame registration, the sharpest frame in the sequence was selected as a reference frame and all other frames registered to it. The registration was carried out using the Matlab function imregister.m, which estimates the affine transformation (consisting of translation, rotation, scale and shear) and aligns all frames with the reference frame.

The vessel filtering proposed in (Jerman et al., 2016_1; Jerman et al., 2016_2) was implemented using Matlab code available in (Jerman,2020). There are three parameters: sigma (vector of scales on which the vesselness is computed), spacing: input image spacing resolution (to adjust the gaussian filter kernel size in each dimension during hessian matrix computation), and tau: a parameter (between 0.5 to 1) that controls response uniformity. A lower tau will result in more intense output response. These three parameters were determined empirically. Sigma was 1:7, spacing 1:1 and tau was set as 1.

The filtered vessel image was converted to a binary image using Otsu's method (Otsu, 1979). The morphological operations were applied to the binary vessel image to extract the centreline of the vessel first, then detect the end and branch points, which can be implemented via Matlab function bwmorph.m options for 'thin', 'endpoints' and 'branchpoints', respectively.

The connected vessel network was broken into individual vessel segments by setting the branch points' neighbouring pixels to zero. Vessel segments longer than 30 pixels were selected for further assessment. An example of the mean of the registered video frames is provided in **Figure 2**, in which the vessel centreline (in red) is overlaid on the vessel network

with the intersection points (in blue). The height for the scale bars is 5 pixels, the length are 10, 20 and 30 pixels, which are 18.1, 36.2 and 54.3μm respectively (based on the conversion rate 1.81 μm/pixel).

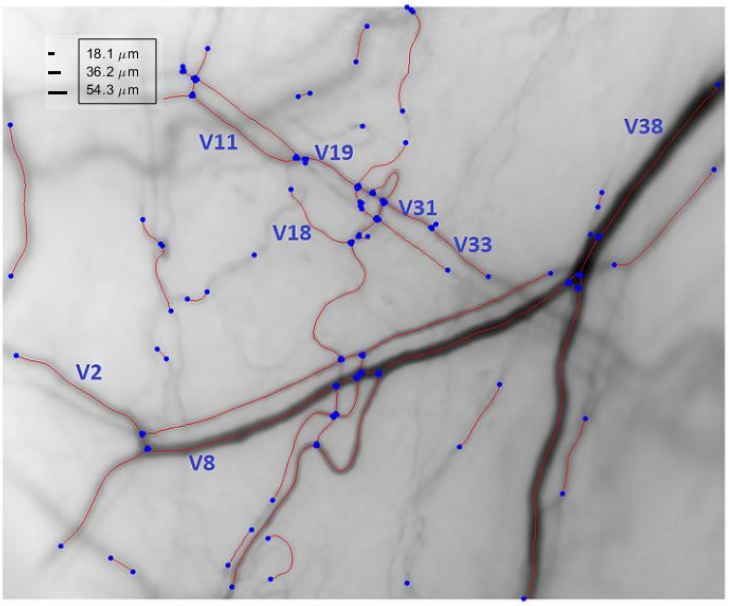

Figure 2. *The mean of the registered image shows the conjunctival microvessel network with scale bars. The vessel centreline (in red) is overlaid on the vessel network with the intersection points (blue).*

2.4. Estimation of Va by 1DTCWT

Va was estimated by applying the 1D+T continuous wavelet transform (1DTCWT) to the Spatial Temporal Image (STI) obtained from the vessel segment. Wavelet transform is an effective tool that can analyse time and frequency information simultaneously. CWT has been applied as a spatio-temporal filter for motion capture for 1D+T signals (Duval-Destin et al., 1993; Wang et al., 2011; Hong et al., 2008) and 2D+T signals (Leduc et al., 1997; Leduc et al., 1996) to achieve moving target tracking. Since the STI signal is the one dimension of space plus time, the approach for 1D+T CWT was selected for Va estimation as illustrated in **Figure 3**. Application of this method included three steps: a) construct the STI for vessel

segment; b) perform 2D fast Fourier transform (2DFFT) and 1DTCWT; c) estimate Va by searching the maximum of the energy map.

2.4.1 Spatial Temporal Image (STI)

The STI can be considered as a time sequence ***I(x,t),*** which denotes the intensity ***I*** at the position *x* in a vessel centreline and the time point *t*. The change of intensity in STI represents the red blood cells (RBCs) flowing through the vessel within the given time (or video frames). An example of STI obtained from V31 (in **Figure 2**) is given in **Figure 3(a)**, in which the x-axis is the number of frames and y-axis is the vessel length in pixels. The motion of RBCs are presented in STI as the dominant bands. The motion tracks can be indicated by a straight line. The slope (pixel/frame) can be calculated by finding two points (x1,y1) and (x2,y2) on the line, so the slope is (y2-y1)/(x2-x1). The slope in STI in **Figure 3(a)** was approximately 4.33 pixel/frame (or 0.47mm/s).

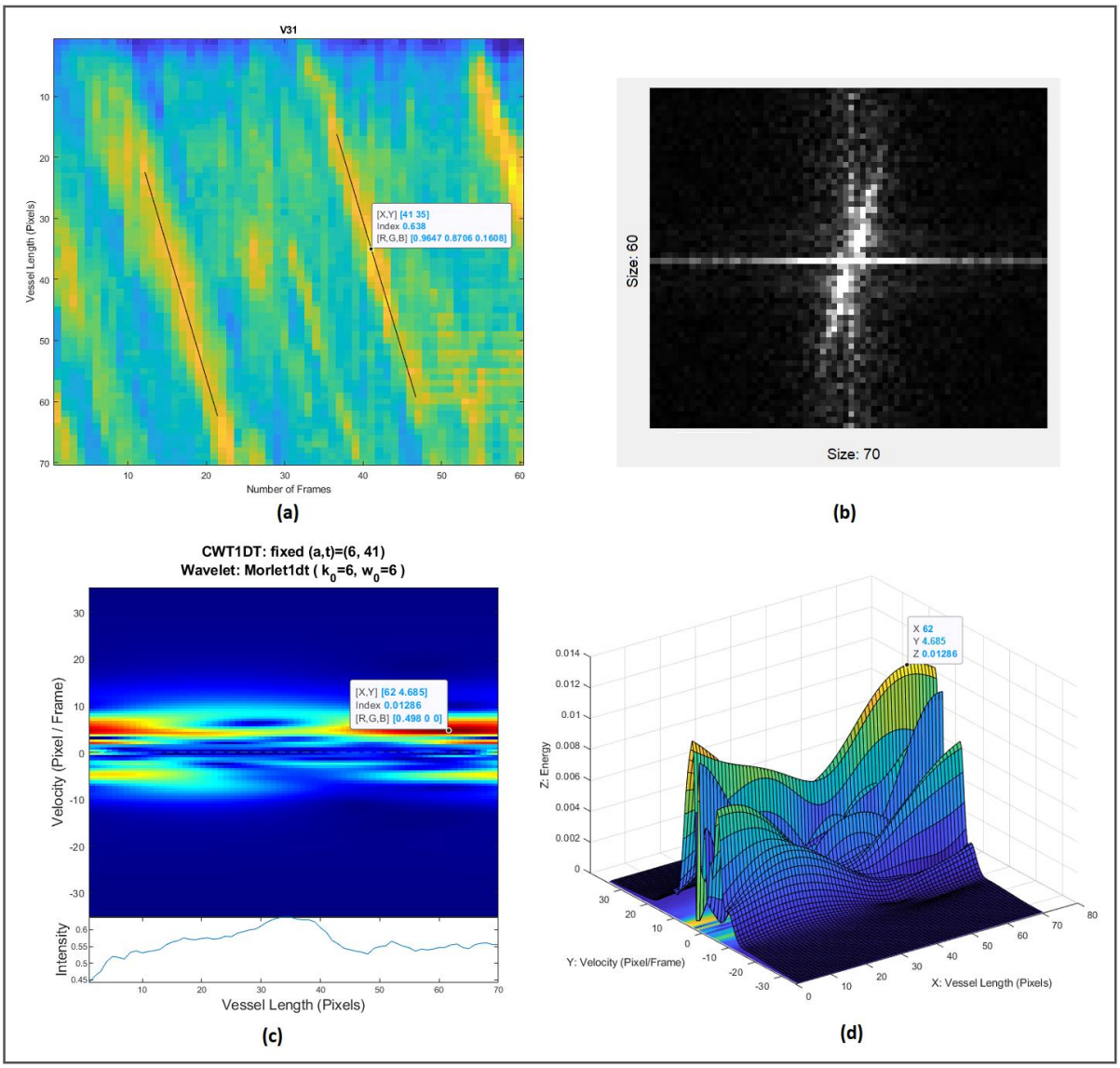

Figure 3. *Examples to demonstrate the proposed approach for estimation of Va by 1DTCWT:* ***(a)*** *STI from vessel V31 (in Figure 2), the RBCs movement is clearly presented in STI and the motion track are indicated by straight lines. [x,y] indicate the position of the selected time point (frame 41) together with intensity;* ***(b)*** *Result after applying 2DFFT to the transpose of STI in (a), which displays the normalised magnitude of 2DFFT and it has the same size as its input;* ***(c)*** *Results after applying 1DTCWT to the outcome of 2DFFT at the selected time point (frame 41). Top: the energy colour map with the information of maximum energy point shown in the box. X: position in the vessel; Y: estimated Va and index for energy value. Bottom: the intensity of STI at frame 41;* ***(d)*** *The 3D surface for the same energy map in* ***(c),*** *which is formed in spatio and velocity spaces together with the energy. The value of energy (in z-axis) corresponds to the index value shown in* ***(c)****.*

2.4.2 Perform 2DFFT and 1DTCWT

The principle behind motion capture is to design the spatio-temporal wavelet to be speed-tuned, then the speed detection is achieved by finding the extremum of an energy function in the spectral domain by means of FFT (Leduc et al., 1997). Given the movement of RBCs within a given time frame, represented by a spatial-temporal signal ***I(x,t),*** the Galilean wavelet referential transformation (Leduc et al., 1997) can be described using:

$$\begin{pmatrix} \vec{x}' \\ t' \\ 1 \end{pmatrix} = \begin{pmatrix} aR(\theta) & \vec{v} & \vec{b} \\ 0 & 1 & \tau \\ 0 & 0 & 1 \end{pmatrix} \begin{pmatrix} \vec{x} \\ t \\ 1 \end{pmatrix} \quad (1)$$

where the symbol $\longrightarrow$ denotes the vector, $\vec{v}$ is the vector of speed; $\vec{b}$ and τ are the spatio-temporal translation, which represent the space and time locations respectively; a is a global dilation to replace the separated dilation in space and time. The spatial rotation $R(\theta)$ can be neglected for 1D+T case. Therefore the operator function on wavelet and signals $[\Omega(\cdot)\Psi](\vec{x},t)$ will include a set of transformation parameters such as:

$$[\Omega(\vec{b},\tau,\vec{v},a)\Psi](\vec{x},t) = \frac{1}{a}\Psi[\frac{1}{a}(\vec{x} - \vec{b} - \vec{v}t), t - \tau] \quad (2)$$

In motion tracking applications, the Morlet wavelet is commonly considered and the corresponding spatio-temporal version is defined as a product of a Morlet wavelet in position and a Morlet wavelet in time. To capture the motion of the spectrum the speed detection is carried in the Fourier space and the Morlet wavelet in frequency domain is performed as:

$$\widehat{\Psi}(\vec{k},\omega) = \left(e^{-\frac{1}{2}|\vec{k}-\overrightarrow{k_0}|^2}\right) \times \left(e^{-\frac{1}{2}(\omega-\omega_0)^2}\right) \quad (3)$$

where $\widehat{\psi}$ denotes the Morlet wavelet in Fourier space, $\vec{k}$ and ω are the spatial and temporal frequencies, respectively. The constant k_0 and ω_0 are defined by the admissibility criterion, which is satisfied when k_0 and $\omega_0 \geq \pi\sqrt{2/\ln 2} \approx 5.336$ (Brault, 2003; Jacques et al., 2001). Therefore, both k_0 and ω_0 were set as 6 in 1DCWT.

2.4.3 Detection of Speed via Searching Local Maximum Energy

Speed detection can be achieved by searching the local maximum of an energy function $E(\vec{b}, \tau, \vec{v}, a)$ formed by the spatio space $\vec{b}$ and velocity space $\vec{v}$. Given a fixed scale $a = a_n$ and a fixed time point $\tau = \tau_i$, where $i = 1,2, \ldots N$, and *N* is the number of frames (x-axis of STI), the energy can be computed from the discretized CWT W_ψ such as:

$$E(\vec{b}, \tau, \vec{v}, a)|_{a=a_n, \tau=\tau_i} = \left|W_\psi(\vec{b}, \tau_i, \vec{v}, a_n)\right|^2 \quad (4)$$

Taking the energy as the function of velocity only as $E(\vec{v})$, along each spatio space b_m, where $m = 1,2, \ldots L$ and *L* is the length of vessel segment (y-axis of STI), the energy at velocity space is obtained by calculating magnitude of $W_\psi(\mathrm{b}_m, \vec{v})$. Speed detection can be achieved by searching the local maximum of the energy function. Note that the CWT was applied at each frame (time point $\tau = \tau_i$) to provide the corresponding velocity. The final Va for STI was based on averaging the absolute value of velocities estimated from all frames. The range of measurable velocity was determined by a predefined velocity space, which was set in a range of [-35,35] (pixel/frame) or [-3.8,3.8] mm/s based on the maximum Va for conjunctival microvessels reported in Khansari et al., 2016.

2.4.4 Implementation of 1DTCWT for Va Estimation

For implementation, we applied the function cwt1dt.m available in MATLAB YAWTb toolbox (Jacques et al., 2001). The parameter setting for k_0 and ω_0 were set as 6 as explained earlier, and a was set as 6 which was determined empirically. Note for function *cwt1dt.m*, the time index varies along the column (vertically), and spatial index is along the row (horizontally). Therefore, 2DFFT was performed on the transpose of STI. The results of applying 2DFFT are provided in **Figure 3 (b),** which displays the normalised magnitude of 2DFFT with the same size as the transpose of STI. For the purpose of demonstration, we selected a point at frame 41 from STI in **Figure 3 (a)** and the results of applying CWT to frame 41 are provided in **Figure 3(c)**. The upper component of **Figure 3(c)** is the energy colour map, in which y-axis represents the velocity space in pixel/frame and x-axis is the spatio space. Estimation of Va was achieved by searching the maximum energy point in the energy map (index value 0.01238). For the point [X,Y], X=62 indicates the position in vessel length, and Y shows the velocity of 4.685 pixel/frame (or 0.50mm/s), which approximates to that found using the "slope" technique in **Figure 3(a)** (approximately 4.33 pixel/frame or 0.47mm/s). The lower component of **Figure 3(c)** presents the intensity of STI at frame 41. The intensity is 0.638 at vessel length 35, is associated with the data point locate in the STI in **Figure 3(a).** In addition, the same energy map is plotted as the 3D surface in **Figure 3(d)**, in which the value of energy (in z-axis) corresponds to the index value shown in **Figure 3(c)**.

More examples of applying 1DCWT to STI from some of selected vessels in **Figure 2** are given in **Figure 4**, which includes the results of V_a (in mm/s) by the proposed method and the "Slope" technique. It can be seen that results from both are comparable.

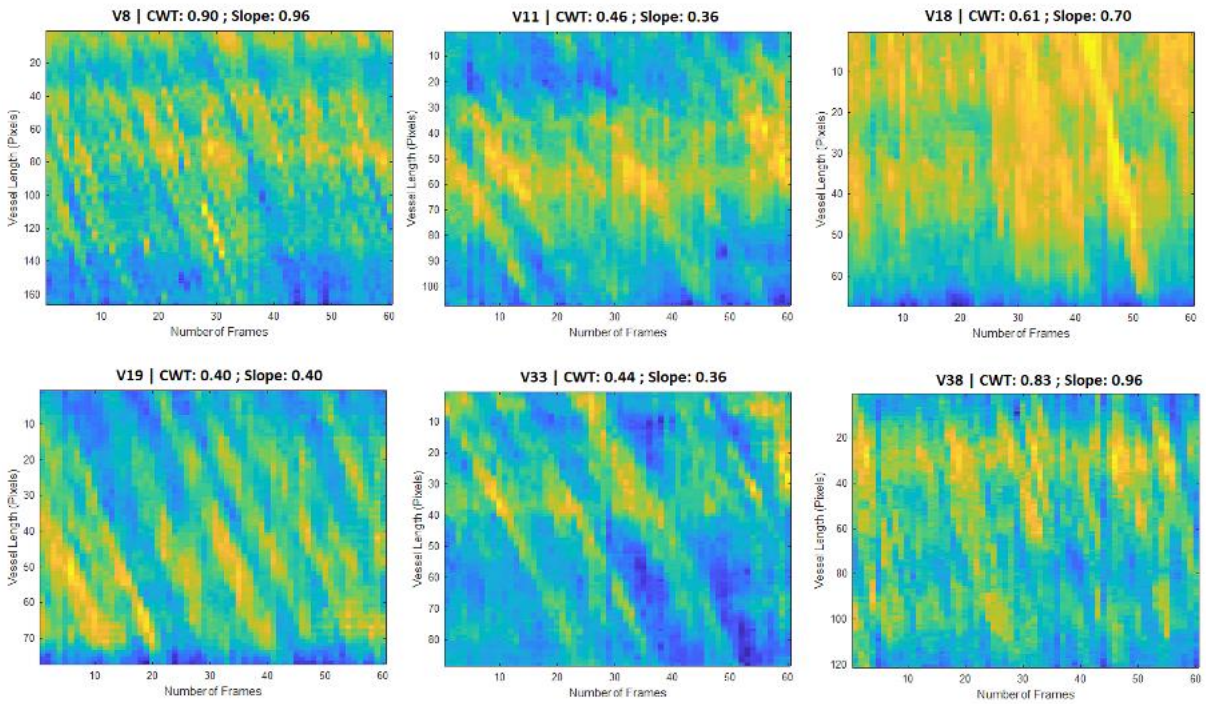

Figure 4. Examples of the STIs from the vessels selected in Figure 2, together with the estimated V_a (in mm/s) by 1DTCWT and the "Slope" technique.

2.5 Calculation of D, Flow Rate (Q) and WSR

The *vessel diameter (D)* was calculated using the Euclidean Distance Transform (EDT) method (Brennan et al., 2019) and vessels were arranged into four groups based on their diameter (D), as previously described (Khansari et al., 2016). The blood volume flow rate (Q) was calculated by the product of the cross-sectional velocity V_s and the cross-sectional area (assuming a circular cross-section): $Q = V_s \frac{\pi D^2}{4}$ and the wall shear rate (WSR) was calculated using V_s values: $WSR = \frac{8V_s}{D}$ (Koutsiaris et al, 2013). For microvessel diameters less than approximately 20 μm, a velocity profile cannot be used in the ordinary sense in order to estimate cross-sectional velocity (Koutsiaris et al., 2013). Therefore, V_s is obtained based on a profile factor function defined in prior work (Koutsiaris, A.G., 2005),

in which the relation between the cross-sectional velocity V_s and axial velocity V_a is derived as:

$$V_s = \begin{cases} V_a & when \;\; D/D_c \leq 0.6, \\ \frac{V_a}{1.58(1-e^{-\sqrt{2D/D_c}})}, & when \;\; D/D_c > 0.6. \end{cases} \quad (5)$$

Where D_c is the size of the average human erythrocyte diameter, that is 7.65μm (Koutsiaris, A.G., 2005). Assessment of repeatability of our methods is described in the **Supplementary file**.

2.6 Statistical analysis

For statistical analysis SPSS for Apple iOS (v.25) was used. Continuous variables were described using the mean, standard deviation (SD) and 95% confidence intervals (CI). The median was applied if the continuous variable was not normally distributed. Kolmogorov-Smirnov testing was used to assess normality of the continuous variables. Categorical variables were expressed as a number and percentage of the total category number to which the variable belonged.

Continuous variables were compared between the two populations using the independent-samples t-test or Mann-Whitney U-test depending on normality.

Categorical comparisons were made using Chi-Square or Fisher's exact test. A one-way analysis of variance or Kruskal-Wallis test was used to compare differences between the two groups based on the vessel groups, followed by post-hoc testing if applicable. Post-hoc analysis included Bonferroni correction or Games-Howell depending on variance assumption.

Assuming a population standard deviation of 1 in the unit of the parameter under study and a difference in mean that exceeds or is equal to +/-1.18, 80% statistical power was deemed achievable at 5% alpha when comparing 11 CCHD patients to 14 controls. Additionally, considering that vessels are the entities being examined for our within vessel group comparisons, and assuming a larger variability in this regard, we can still achieve high power (91%) considering a wider standard deviation of 6, with a difference between groups that exceeds or is equal to 1.5 (Dupont et al., 1990).

An α-level of less than 0.05 was determined to be of statistical significance. Conjunctival vessel sizes are heterogeneous and we applied a grouping system (Khansari et al., 2016) based on diameter i.e. group 1 (D<11μm), 2 (D 11-16μm), 3 (D 16-22μm) and 4 (D>22μm).

Comparisons between the two study groups were made at two levels. Firstly, we averaged all the vessel segment measurements (D, Va, Q and WSR) for each participant obtaining 11 and 14 overall values for the CCHD and controls, respectively. Secondly, as Va has been shown to be positively correlated with D (Khansari et al., 2016; Brennan et al., 2019) we compared the measurements within each vessel group (1-4, as above) which removes any confounding factor for differences in diameter. For this we used the average of each conjunctival measurement across all vessel segments (736 segments in total, 292 CCHD vs 444 healthy recruits) in each study group to counteract the heterogeneous distribution of vessel sizes.

3 Results

3.1 Population

11 patients with CCHD and 14 healthy controls were recruited. The mean age of the CCHD patients was 35 ± 12 years compared to 40 ± 9 years for the controls (p=0.25). Sex distributions were similar between the two groups with females representing 36% (n=4) of the CCHD patients and 36% (n=5) of the controls.

Right heart obstruction with reduced pulmonary blood flow was the dominant defect (n=7, 64%) in the CCHD patients. CCHD defects are listed in **Table 1.**

Table 1. Classification of CCHD defect based on pulmonary blood flow.

Decreased pulmonary blood flow	**n=7**
Pulmonary atresia/VSD	5
Tricuspid atresia	1
Double-inlet left ventricle/pulmonary stenosis	1
Increased pulmonary blood flow	**n=4**
Double-outlet right ventricle/transposition of great arteries	1
Partial anomalous pulmonary venous drainage	1
Left atrial isomerism/common AV valve/bilateral SVC/VSD	1
Double-inlet left ventricle/PDA/VSD	1
Total	**n=11**

CCHD- Cyanotic congenital heart disease. VSD- Ventriculoseptal defect. AV- Atrioventricular. SVC- Superior vena cava. PDA- Patent ductus arteriosus.

The CCHD group were markedly hypoxic with a mean SpO_2 of 84 ±10% (p= 0.001). There were no significant differences in resting heart rate or systolic blood pressure. The CCHD group had a lower mean diastolic blood pressure compared to the control group (68 ±13mmHg vs 79 ±14 mmHg, p=0.06) likely reflective of underlying structural cardiac disease and prescribed vasoactive drugs, as summarised in **Table 2**. The CCHD patients were erythrocytotic with a mean plasma haemoglobin level 186 ±25g/L and haematocrit 56 ±1%. The CCHD patients also had significantly raised NT-proBNP levels (1518 ±1487g/L) due to chronic heart failure and underlying heart disease. Baseline serum urate was higher in the CCHD patients compared to the controls (0.51 ±0.21mg/dL vs 0.31 ±0.09mg/dL, p=0.02).

Table 2 Baseline clinical, laboratory and pharmacotherapy characteristics.

Clinical characteristic	**Control (n=14)**	**Cyanotic ACHD (n=11)**	**p value**
Age, years ±SD	40 ±9	35 ±12	0.25
Female, n (%)	5 (36)	4 (36)	1.00
Oxygen saturations, (%)	98	84	**0.001**
Pulse rate, bpm ±SD	70 ±10	79 ±15	0.12
SBP, mmHg ±SD	126 ±23	122 ±15	0.69
DBP, mmHg ±SD	79 ±14	68 ±13	0.06
Haemoglobin, g/L ±SD	146 ±7	186 ±25	**<0.001**
Platelet count, $x10^3$ ±SD	278 ±33	166 ±44	**<0.001**
Haematocrit, ±SD	0.43 ±0.03	0.56 ±0.1	**<0.001**
NT-pro BNP, ng/L ±SD	30 ±33	1518 ±1487	**0.01**
Urate, mg/dL ±SD	0.31 ±0.09	0.51 ±0.21	**0.02**
Creatinine clearance, mL/min ±SD	105 ±36	89 ±56	0.43
CRP, mg/L ±SD	1.7	8	0.17
Aspirin, n (%)	0	2 (18)	n/a
Oral anticoagulation, n (%)	0	6 (55)	n/a
Phosphodiesterase inhibitor, n (%)	0	7 (64)	n/a
Endothelin receptor antagonist, n (%)	0	4 (36)	n/a
Prostacyclin analogue, n (%)	0	1 (9)	n/a

SD- Standard deviation. SBP- Systolic blood pressure. DBP- Diastolic blood pressure. NT-proBNP- N terminal pro brain natriuretic peptide. CRP- C reactive protein. n/a- Not applicable.

3.2 Conjunctival microcirculation assessment

Conjunctival videos were captured for all patients with no reported adverse events. Image processing and analysis was performed in an independent laboratory within our affiliated institutions, blind to the patient's history.

There was no significant difference in vessel diameter (20.2 ±2.6μm CCHD vs. 20.4 ±2.7μm controls, p=0.86). Axial velocity (Va) was lower in the CCHD group (0.47 ±0.06mm/s CCHD vs 0.53 ±0.05mm/s controls, p=0.03). Blood volume flow (Q) was lower in the CCHD group but this was not statistically significant (121 ±30pl/s CCHD vs 145 ±50fl/s controls, p=0.65). Wall shear rate (WSR) was found to be significantly lower in the CCHD group (153 ±27s^{-1} CCHD vs 174 ±22s^{-1} controls, p=0.04). **Table 3** summarises these results.

Table 3 Comparisons of conjunctival microcirculatory parameters.

Parameter measured	Controls (n=14)	CCHD (n=11)	p value
D (μm) ±SD	20.2±2.6 Range (5.8-58.1) IQR (13.8-26.1)	20.4 ±2.7 Range (7-48) IQR (15.1-26.3)	0.86
Va (mm/s) ±SD	0.53 ±0.05 Range (0.16-0.96) IQR (0.42-0.62)	0.47 ±0.06 Range (0.03-0.93) IQR (0.40-0.58)	**0.03**
Q (pl/s) ±SD	145 ±50 Range (7-1178) IQR (50-206)	121 ±30 Range (4-842) IQR (60-177)	0.65
WSR (s^{-1}) ±SD	174 ±22 Range (40-734) IQR (111-200)	153 ±27 Range (9-640) IQR (92-192)	**0.04**

CCHD- Cyanotic congenital heart disease. D- Diameter. Va- Axial velocity. Q- Blood flow. WSR- Wall shear rate. SD- Standard deviation. IQR- Interquartile range.

Using the aforementioned vessel groups (1-4), we compared each conjunctival measurement for the two groups using the average of all 736 vessel segments (292 CCHD, 27 per patient vs 444 controls, 32 per control).

44% (326/736) of vessels fell within the group 4 diameter range (> 22μm) and were the most frequently observed vessels. Va did not differ significantly between the two populations for vessel groups 1-3. In group 4 vessels Va was lower in the CCHD patients (0.50 $\pm$0.16mm/s vs 0.58$\pm$0.15, p <0.001).

Q did not differ significantly for group 1 or 3 vessels. Q was found to be higher in CCHD patients in group 2 vessels (56 $\pm$19pl/s vs 49 $\pm$18, p=0.04) but in group 4 the opposite of this was found with Q being lower in CCHD patients (216 $\pm$121 vs 258 $\pm$154, p=0.001).

WSR was consistently lower in the CCHD patients for all vessel groups and the most substantial differences were found in group 4 vessels (100 $\pm$35 vs 115 $\pm$33,

p <0.001). **Figure 5** illustrates the differences in mean Va, Q and WSR for group 4 vessels.

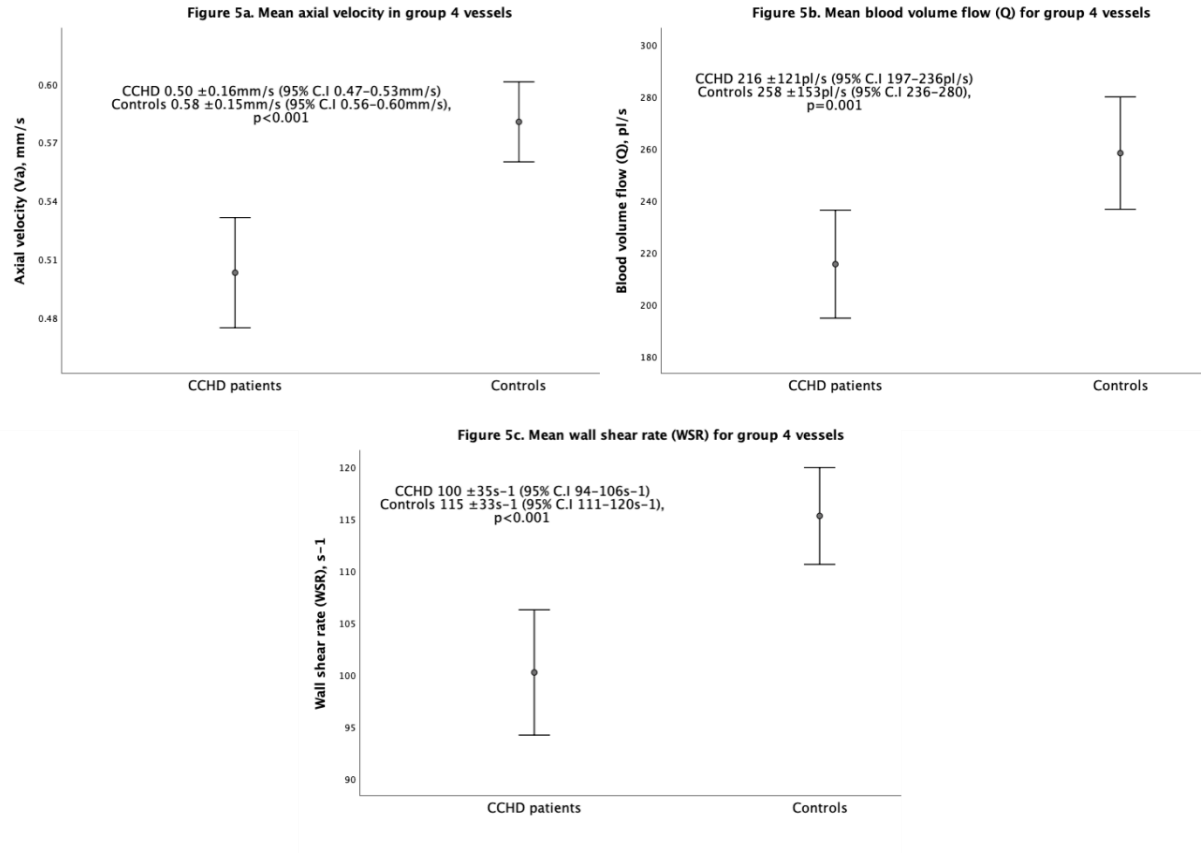

Figure 5. *Comparisons between both CCHD patients and controls for group 4 (>22μm) of (a) Mean axial velocity (Va), (b) Mean blood volume flow (Q) and (c) Mean wall shear rate (WSR).*

Table 4 is a comparison summary of the conjunctival measurements based on vessel group size.

Table 4. Summary of conjunctival microcirculatory parameters grouped by vessel size.

Parameter measured	**Controls (n=14)**	**CCHD (n=11)**	**p value**
Group 1 (<11μm)	**Number of vessels 52**	**Number of vessels 32**	
D, μm ±SD (range)	8.9 ±1.4 (5.8-10.9)	9.2 ±0.1 (7-11)	0.54
Va, mm/s ±SD (range)	0.48 ±0.13 (0.21-0.81)	0.44 ±0.16 (0.11-0.82)	0.38
Q, pl/s ±SD (range)	25 ±10 (7-51)	24 ±10 (4-45)	0.69
WSR, s^{-1} ±SD (range)	366 ±123 (131-734)	314 ±120 (74-640)	0.06
Group 2 (11-16μm)	**Number vessels 95**	**Number vessels 52**	
D, μm ±SD (range)	13.2±1.4 (11-15.7)	13.9 ±1.3 (11.3-16)	**0.01**
Va, mm/s ±SD (range)	0.47 ±0.13 (0.16-0.80)	0.49 ±0.13 (0.17-0.76)	0.37
Q, pl/s ±SD (range)	49 ±18 (15-103)	56 ±19 (24-91)	**0.04**
WSR, s^{-1} ±SD (range)	213 ±62 (79-382)	209 ±57 (64-380)	0.74
Group 3 (16-22μm)	**Number vessels 102**	**Number vessels 77**	
D, μm ±SD (range)	18.8 ±1.9 (16-21.9)	19.3 ±1.8 (16-22)	0.11
Va, mm/s ±SD (range)	0.49 ±0.12 (0.16-0.82)	0.49 ±0.16 (0.03-0.81)	0.87
Q, pl/s ±SD (range)	98 ±33 (41-193)	102 ±40 (5-209)	0.29
WSR, s^{-1} ±SD (range)	149 ±39 (40-257)	144 ±48 (9-239)	0.41
Group 4 (>22μm)	**Number vessels 195**	**Number vessels 131**	
D, μm ±SD (range)	28.1 ±5.7 (22-58)	27.8 ±4.4 (22-48)	0.59
Va, mm/s ±SD (range)	0.58 ±0.15 (0.21-0.96)	0.50 ±0.16 (0.08-0.93)	**<0.001**
Q, pl/s ±SD (range)	258 ±154 (57-1179)	216 ±121 (31-842)	**0.001**
WSR, s^{-1} ±SD (range)	115 ±33 (44-196)	100 ±35 (15-180)	**<0.001**

D- Diameter. Va- Axial velocity. Q- Blood flow. WSR- Wall shear rate. SD- Standard deviation. CCHD- Cyanotic congenital heart disease

4 Discussion

We non-invasively evaluated the conjunctival microcirculation in a group of patients with CCHD compared to a matched group of healthy controls. This was performed safely. We found important differences between these physiologically very contrasting groups. Due to chronic hypoxia, the CCHD patients were erythrocytotic, as evidenced by their haemoglobin and haematocrit elevations. This is a secondary physiological response to chronic tissue hypoxia leading to rises in serum erythropoietin concentrations and secondary erythropoiesis causing increased haematocrit, red cell mass and haemoglobin to improve the oxygen-carrying capacity of blood(Spence et al., 2007; Rosove et al., 1986; Warrell et al., 2003; Territo et al, 1991; Murray et al, 1963; Franke et al., 2013). This can result in hyperviscosity and a subsequent reduction in blood flow and red cell velocity (Kontras et al., 1970). These changes are associated with microvascular and endothelial dysfunction, manifest by impaired vascular tone and vasoreactivity (De Stefano et al., 2008; Vianello et al, 2015). This dysfunction, alongside the circulatory hyperviscosity, is associated with increased risk for adverse vascular events, such as stroke and pulmonary emboli (PE) (Engelfriet et al, 2005).

The CCHD patients also had, as reported in prior studies, abnormally raised serum NT-proBNP (Baggen et al., 2018) and urate concentrations, reflective of underlying structural heart disease (Wannamethee et al., 2018; Hayabuchi et al., 1993). The baseline clinical observations (pulse rate, systolic blood pressure) were similar between the two groups, increasing confidence that any observed differences are on account of chronic hypoxia.

A large number of vessels (n=736) were analysed. Overall there were no significant differences in vessel diameters between the two groups. Prior studies evaluating the conjunctival microcirculation in patients with sickle cell disease (Kord Valeshabad et al., 2014), a condition typically associated with retinal microvascular abnormalities (Acacio et al., 1973), and patients with diabetic retinopathy (Khansari et al., 2017) also found no significant differences in diameter between the study groups suggesting a vascular remodelling effect with chronic microcirculatory dysfunction.

Mean Va was lower in CCHD patients compared to healthy controls. This was most pronounced for the most commonly encountered vessel size i.e. group 4 (diameter > 22μm). Lower Va has also been reported in studies assessing the conjunctival microcirculation for diabetic (Khansari et al., 2017; Cheung et al., 2001), sickle cell retinopathy (Kord Valeshabad et al., 2014) and post unilateral ischaemic stroke patients (Kord Valeshabad et al., 2015). Lower Va, as observed for CCHD patients in our study, appears to occur in patients with established cardiovascular disease and may be a candidate marker of microcirculatory dysfunction. This may have potential for application to cardiovascular disease assessment and screening.

Mean Q did not differ significantly, overall, between the two groups. Q was, however, lower in the CCHD patients for group 4 vessels which were the most frequently analysed vessels. This reduction in Q may indicate endothelial dysfunction due to chronic hypoxia and secondary erythrocytosis though further studies are required to provide improved understanding of this finding. Interestingly, Q was found to be higher in CCHD patients in group 2 vessels and this possibly reflects a combination of limited sample size and vessel differentiation e.g. it is possible in group 2 that more of the vessels are arterioles.

Reduced WSR is a marker of endothelial dysfunction and alterations in WSR have been found in prior studies of patients with cardiovascular disease (Jiang et al., 2000). Lower wall shear stress (WSS), a product of WSR and plasma viscosity, has previously been associated with upregulation of hypoxia-inducible factor 1 α (HIF1α) and tissue hypoxia (Feng et al., 2017) in porcine and murine arteries. Reductions in WSS are seen in conditions with reduced flow or flow turbulence (Papaioannou et al., 2005) and have been reported in patients with aortic aneurysm (Raghavan et al., 2000) and congenital subaortic stenosis (Cape et al., 1997; Gerrah et al., 2017). We reported a significantly lower overall mean WSR for the CCHD patients, again with the most significant differences observed for group 4 vessels (the most prevalent). WSR has a potential role in evaluating endothelial function and pathophysiology (Koutsiaris et al., 2015; Brennan et al., 2019). The lower WSR observed for the CCHD patients, like the reductions in Va and Q (group 4 vessels), may be a secondary response to chronic tissue hypoxia and erythrocytosis. Further study is required to explore and better understand our findings.

Our study has limitations including not differentiating vessels into venules or arterioles. For example, group 4 vessels were the most frequently analysed vessels and had the most pronounced reductions in Q, Va and WSR. Vessel differentiation could, therefore, help explain the differences between the groups further. Prior studies have reported vessel differentiation using manual identification based on flow principles i.e. blood travelling from a vessel into a larger vessel is a venule and vice-versa for arterioles (Khansari et al., 2016; Koutsiaris et al., 2007). Vessel differentiation was not possible within the confines of this pilot study but it warrants further exploration. Va values were limited to 1mm/s and this is

reflective of our current technical methodology which is addressed in the **supplementary file.**

Our study of 25 individuals, with 736 vessels analysed, is small but was sufficient for statistical comparisons as described in our methods section. Our study size in practical terms is also reflective of the prevalence of adults with CCHD living within our catchment area. All patients were recruited from the Belfast Health and Social Care Trust, the tertiary referral centre for congenital heart disease in Northern Ireland.

5 Conclusions

Conjunctival microvascular and endothelial function assessment using a slit-lamp biomicroscope and iPhone 6s found reduced Va and WSR in CCHD patients compared to healthy controls. In larger conjunctival microvessels, a reduction in blood volume flow (Q) was also found. These changes are suggestive of a microvascular response to chronic hypoxia and secondary erythrocytosis. Such assessments may have a role in the evaluation of patients with CCHD and other causes of hypoxia and erythrocytosis.

6 Funding

This project was funded by the Heart Trust fund, Royal Victoria Hospital, Belfast; the Regional Medical Cardiology Centre (RMCC), Royal Victoria Hospital, Belfast; Northern Ireland Chest Heart and Stroke (NICHS) and the Ulster University located in Northern Ireland, United Kingdom. The work for image processing and microcirculatory parameters estimation was part-funded by Interreg SEUPB funding associated with Eastern Corridor for Medical Engineering (ECME).

7 Declaration of Competing Interest.

The authors have no conflicts of interest or anything to disclose with respect to this original research manuscript.

8 Data availability

The datasets for the current study are available from the corresponding author on reasonable request.

9 References

Acacio I, Goldberg M., 1973. Peripapillary and macular vessel occlusions in sickle cell anemia. American journal of ophthalmology, co5):861–866.

Baggen V, Baart S, Van den Bosch A, et al., 2018. Prognostic Value of Serial N-Terminal Pro-B-Type Natriuretic Peptide Measurements in Adults With Congenital Heart Disease. J Am Heart Assoc, 7(7): e008349.

Baumgartner H, Bonhoeffer P, De Groot N et al., 2010. ESC Guidelines for the management of grown-up congenital heart disease (2010). European Heart Journal, 31(23):2915-2957.

Brault P., 2003. Motion estimation and video compression with spatio-temporal motion-tuned wavelets. WSEAS Transactions on Mathematics2, 4:67-78.

Brennan P, et al., 2019. Quantitative assessment of the conjunctival microcirculation using a smartphone and slit-lamp biomicroscope. Microvascular Research,*126* (C). https://doi.org/10.1016/j.mvr.2019.103907.

Cape E, Vanauker M, Sigfusson G, Tacy T, del Nido P., 1997. Potential role of mechanical stress in the etiology of pediatric heart disease: septal shear stress in subaortic stenosis. *J* Am Coll Cardiol, 30(1):247–54.

Cheung A, et al., 2001. Microvascular abnormalities in the bulbar conjunctiva of patients with type 2 diabetes mellitus. Endocrine Practice, 7(5):358-363.

Cordina R, Leaney J, Graham S, Celermajer D, Golzan M, Grieve S., 2015. Ophthalmological consequences of cyanotic congenital heart disease: vascular parameters and nerve fibre layer. Clinical and Experimental Ophthalmology, 43: 115–123.

Cordina R, Nakhla S, O'Meagher S, Leaney J, Graham S, Celermajer D., 2015_2. Widespread endotheliopathy in adults with cyanotic congenital heart disease. Cardiology in the Young, 25(3), 511–519.

De Stefano V, Za T, Rossi E, et al., 2008. Recurrent thrombosis in patients with polycythemia vera and essential thrombocythemia: Incidence, risk factors, and effect of treatments. Haematologica, 93(3):372–380.

Dupont WD, Plummer WD., 1990. Power and Sample Size Calculations: A Review and Computer Program. Controlled Clinical Trials, 11:116-28.

Duval-Destin M, Murenzi R., 1993. Spatio-Temporal Wavelet: Application to the Analysis of Moving Patterns, in Progress in Wavelets Analysis and Applications. FrontiReres, Gif-sur-Yvette:399-408.

Engelfriet P, Boersma E, Oechslin E, et al., 2005. The spectrum of adult congenital heart disease in Europe: morbidity and mortality in a 5 year follow-up period. The Euro Heart Survey on adult congenital heart disease. Eur Heart J, 26(21): 2325–2333.

Feng S, Bowden N, Fragiadaki M, et al., 2017. Mechanical Activation of Hypoxia-Inducible Factor 1α Drives Endothelial Dysfunction at Atheroprone Sites. Aterioscler Thromb Vasc Biol,37*(*11):2087-2101.

Franke K, Gassman M, Wielockx B., 2013. Erythrocytosis: the HIF pathway in control. Blood, 122(7):1112-1128.

Gerrah R, Haller S, George I., 2017. Mechanical Concepts Applied in Congenital Heart Disease and Cardiac Surgery. Ann Thorac Surg,103(6):2005-14.

Hayabuchi Y, Matsuoka S, Akita H, Kuroda Y., 1993. Hyperuricaemia in cyanotic congenital heart disease. Eur J Pediat, 152(11):873-876.

Hong L, Ruan Y, Li W, Wicker D, Layne J., 2008. Energy-based video tracking using joint target density processing with an application to unmanned aerial vehicle surveillance. Computer Vision, IET, 2(1):1-12.

Jacques L, Coron A, Vandergheynst P, Rivoldini A., 2001. The YAWTb toolbox: Yet another wavelet toolbox. 2001. https://sites.uclouvain.be/ispgroup/yawtb/doc/

Jerman T, Pernus F, Likar Z, Spiclin Z., 2016_1. Enhancement of vascular structures in 3D and 2D angiographic images. IEEE Trans. Med. Imaging 35 (9), 2108–2118.

Jerman T, Pernus F, Likar Z, Spiclin Z., 2016_2. "Blob Enhancement and Visualization for Improved Intracranial Aneurysm Detection", IEEE Transactions on Visualization and Computer Graphics, 22(6), p. 1705-1717.

Jerman T (2020). Jerman Enhancement Filter (https://github.com/timjerman/JermanEnhancementFilter), GitHub. Accessed December 2020.

Jiang Y, Kohara K, Hiwada K., 2000. Low wall shear stress in carotid arteries in subjects with left ventricular hypertrophy. American J Hypertension, 13(8):892-898.

Khansari et al., 2017. Assessment of Conjunctival Microvascular Hemodynamics in Stages of Diabetic Microvasculopathy. Sci Rep, 7:45916.

Khansari M, Wanek J, Felder A, Camardo N, Shahidi M., 2016. Automated assessment of hemodynamics in the conjunctival microvasculature network. IEEE Transactions on Medical Imaging, 35(2):605-611.

Khansari, M.M., Tan, M., Karamian, P. and Shahidi, M., 2018. Inter-visit variability of conjunctival microvascular hemodynamic measurements in healthy and diabetic retinopathy subjects. Microvascular research, 118, pp.7-11.

Kontras S, Bodenbender J, Craenen J, Hosier D., 1970. Hyperviscosity in congenital heart disease. J Pediatr, 76(2):214–20.

Kord Valeshabad A, Wanek J, Mukarram F, Zelkha R, Testai FD, Shahidi M., 2015. Feasibility of Assessment of Conjunctival Microvascular Hemodynamics in Unilateral Ischemic Stroke. Microvasc Res, 100:4–8.

Kord Valeshabad A, Wanek J, Zelkha R, Lim J, Camardo N, Gaynes B, Shahidi M., 2015. Conjunctival microvascular haemodynamics in sickle cell retinopathy. Acta Ophthalmol, 93(4):275-80.

Koutsiaris AG, Tachmitzi S, Papavasileiou P, Batis N, Kotoula M, Giannoukas A, Tsironi E., 2010. Blood velocity pulse quantification in the human conjunctival pre-capillary arterioles. Microvasc Research, 80(2):202-8.

Koutsiaris AG, Tachmitzi S, Batis N., 2013. Wall shear stress quantification in the human conjunctival pre-capillary arterioles in vivo. Microvascular Research, 85: 34-39.

Koutsiaris, A.G., 2005. Volume flow estimation in the precapillary mesenteric microvasculature in vivo and the principle of constant pressure gradient. Biorheology, 42(6):479-491.

Koutsiaris AG., 2015. Wall shear stress in the human eye microcirculation in vivo, segmental heterogeneity and performance in vitro. Clinical hemorheology and microcirculation, 63(1):15-33.

Koutsiaris A, et al. 2007. Volume flow and wall shear stress quantification in the human conjunctival capillaries and post-capillary venules in vivo. Biorheology, 44(5): 375–386.

Leduc JP, Mujica F, Murenzi R, Smith M., 1997. Spatio-temporal wavelet transforms for motion tracking. In Acoustics,Speech, and Signal Processing, 1997. ICASSP-97., 1997 IEEE International Conference, 4:3013-3016 .

Leduc JP, Labit C., 1996. Spatio-Temporal Wavelet Transforms for Image Sequence Analysis. VIII European Signal Processing Conference,EUSIPCO-96:1-4.

MacKenzie L, Choudhary T. McNaught A, Harvey A., 2016. In vivo oximetry of human bulbar conjunctival and episcleral microvasculature using snapshot multispectral imaging. Exp Eye Res, 149:48-58.

Moka S, Koutsiaris A, Garas A, Messinis I, Tachmitzi S, Giannoukas A, Tsironi E.,2020. Blood flow velocity comparison in the eye capillaries and postcapillary venules between normal pregnant and non-pregnant women. Microvascular Research, 127:103926.

Moons P, Bovijn L, Budts W, Belmans A, Gewillig M., 2010. Temporal Trends in Survival to Adulthood Among Patients Born With Congenital Heart Disease From 1970 to 1992 in Belgium. Circulation, 122(22):2264-2272.

Mulder B., 2012. Epidemiology of adult congenital heart disease: demographic variations worldwide. Neth Heart Journal, 20(12):505-508.

Murray J, Gold P, Johnson B., 1963. The circulatory effects of hematocrit variations in normovolemic and hypervolemic dogs. J Clin Invest, 42:1150–9.

Otsu, “A threshold selection method from gray-level histograms.” IEEE transactions on systems, man, and cybernetics 9, no. 1, pp.62-66, 1979.

Papaioannou T, Stefanadis C., 2005. Vascular wall shear stress:basic principles and methods. Hellenic J Cardiol, 46(1):9–15.

Raghavan M, Vorp D, Federle M, Makaroun M, Webster M., 2000. Wall stress distribution on three-dimensionally reconstructed models of human abdominal aortic aneurysm. J Vasc Surg, 31(4):760–9.

Rosove M, Hocking W, Child J, et al., 1986. Chronic hypoxaemia and decompensated erythrocytosis in cyanotic congenital heart disease. Lancet, 2(8502):313-315.

Schaan C, Feltez G, Schaan B, Pellanda L., 2019. Functional capacity in children and adolescents with congenital heart disease. Rev Paul Pediatr, 37(1):65-72.

Shahidi M, Wanek J, Gaynes B, Wu T., 2010. Quantitative assessment of conjunctival microvascular circulation of the human eye. Microvasc Research, 79(2):109-13.

Spence M, Balaratnam M, Gatzoulis M, 2007. Clinical Update: cyanotic adult congenital heart disease. Lancet, 9598(370):1530-1532.

Territo M, Rosove M., 1991. Cyanotic congenital heart disease: hematologic management. J Am Coll Cardiol.18(2):320–2.

Tsui I, Shamsa K, Perloff J, Wirthlin R, Schwartz S., 2009. Retinal Vascular Patterns in Adults with Cyanotic Congenital Heart Disease. Seminars in Ophthalmology, 24(6):262-5.

Vianello F, Cella G, Osto E, et al., 2015. Coronary microvascular dysfunction due to essential thrombocythemia and policythemia vera: The missing piece in the puzzle of their increased cardiovascular risk? Am J Hematology, 90(2):109-113.

Waldman J, Wernly J., 1999. Cyanotic congenital heart disease with decreased pulmonary blood flow in children. Pediatr Clin North Am, 46(2):85-404.

Wang R, Zhao Y, Tang Y, Yuan Y., 2011. A spatio-temporal filtering method for motion estimation. The 6th International Conference on Computer Science and Education (ICCSE), ThC 6.3:830-834.

Wannamethee S, Papacosta O, Lennon L, Whincup P., 2018. Serum uric acid as a potential marker for heart failure risk in men on antihypertensive treatment: The British Regional Heart Study. Int J Cardiol, 252:187-192.

Warrell D, Cox T, Firth J, Benz E., 2003. Cyanotic Heart Disease: A Multisystem Disorder. Oxford Textbook of Medicine, 4th edition. London: Oxford University Press; 2003